

Short-range order and Fe clustering in $\text{Mg}_{1-x}\text{Fe}_x\text{O}$ under high pressureI. Kantor,^{*} L. Dubrovinsky, C. McCammon, G. Steinle-Neumann, and A. Kantor
Bayerisches Geoinstitut, Bayreuth University, 95440 Bayreuth, Germany

N. Skorodumova

Condensed Matter Theory Group, Uppsala University, 75105 Uppsala, Sweden

S. Pascarelli and G. Aquilanti

European Synchrotron Radiation Facility, 38043 Grenoble, France

(Received 23 November 2008; revised manuscript received 3 May 2009; published 29 July 2009)

By combining high-pressure and high-temperature Mössbauer spectroscopic studies of (Mg,Fe)O with results of *ab initio* simulations, several important properties of this material were established. Under high pressure (Mg,Fe)O shows changes in the short-range order with the tendency to form iron clusters. These changes were found to be irreversible, implying sluggish kinetics of these processes at ambient conditions. The pressure-induced spin crossover is interpreted here as a gradual noncooperative transition. The onset and width of spin crossover depends, therefore, not only on pressure, temperature, and composition, but also on short-range order in the FeO-MgO solid solution.

DOI: [10.1103/PhysRevB.80.014204](https://doi.org/10.1103/PhysRevB.80.014204)

PACS number(s): 61.50.Ks, 75.30.Wx, 33.45.+x, 81.30.Hd

I. INTRODUCTION

The (Mg,Fe)O solid solution has been the subject of numerous recent studies, both experimental and theoretical.¹⁻⁵ Magnesium-rich (Mg,Fe)O (mineral name ferropericlase) is one of the most important phases for earth sciences since it forms a significant part of the earth's lower mantle and is probably the most abundant simple oxide within the Earth.⁶ Many recent studies focus on the pressure-induced spin crossover of Fe^{2+} in this material and the consequences of the electronic transition on elasticity, density, transport properties, etc. The endmember FeO shows interesting physical behavior, caused by the presence of unpaired *d* electrons and their interactions such as antiferromagnetic ordering,⁷ high-pressure polymorphism,⁸ and possible spin-pairing transition.⁹ FeO is also a strongly correlated material and is often used as a test compound for different *ab initio* techniques that aim to include the effect of electronic correlations in the model.¹⁰⁻¹² In contrast, MgO is one of the simplest oxides, and its properties can be calculated with high accuracy within the conventional approximations of density-functional theory.¹³ The effect of dissolving FeO in MgO is therefore interesting not only for earth sciences, but also for fundamental physics.

Every solid solution or alloy is characterized not only by its composition, but also by the relative positions of its elements, distributed over one or more crystallographic sites. Two components can form either a random (completely disordered) solution, or a solution with some degree of long-range or short-range ordering. The effects of long-range order (LRO) and short-range order (SRO) have been studied in detail in many metallic alloys systems, starting from the classical work of Cowley.¹⁴ Atomic ordering affects many physical properties of the material. SRO can be easily studied experimentally in the case when mixing atoms occupy two or more nonequivalent positions and is directly coupled to the long-range order. In such a case the relative populations of different structural sites can be determined using a number of

conventional methods, in particular x-ray diffraction, Mössbauer or optical spectroscopy, NMR, etc. Typical examples of such systems are the silicate mineral olivine $(\text{Mg,Fe})_2\text{SiO}_4$ and orthopyroxene $(\text{Mg,Fe})\text{SiO}_3$, where there are two slightly different octahedral sites M1 and M2, and the distribution of Fe/Mg between these positions changes with temperature.^{15,16} If two or more components occupy one crystallographic position, only experimental methods sensitive to the local atomic environment can be used to study SRO, which makes the experimental observation of short-range cation ordering more difficult.

Up to now, (Mg,Fe)O has always been regarded as a fully disordered solid solution with no SRO. Indeed, (Mg,Fe)O at ambient pressure shows continuous miscibility and no evidence for any tendency to form ordered structural compounds has ever been observed. Waychunas *et al.*¹⁷ showed the absence of SRO in (Mg,Fe)O samples of different compositions synthesized at ambient pressure and high temperatures, based on a combined extended x-ray absorption spectroscopy (EXAFS) and Mössbauer spectroscopic study. However, at high pressures the situation can be different. There is experimental evidence for the decomposition of (Mg,Fe)O into Fe-rich and Mg-rich components in the laser-heated diamond-anvil cell, implying the appearance of a miscibility gap under high pressure.^{18,19} The existence of a miscibility gap means that Fe ions tend to separate from Mg ions, and therefore under high-pressures SRO in (Mg,Fe)O solid solutions could deviate from a random distribution, with a tendency toward Fe clustering. This manuscript presents the results of an experimental and theoretical study of $(\text{Mg}_x\text{Fe}_{1-x})\text{O}$ solid solutions with $x=0.8-0.95$ in order to establish the actual SRO in ferropericlase under high pressure and its effect on the pressure-induced spin crossover.

II. EXPERIMENTAL DETAILS

Three ferropericlase samples were used in this study, containing 5, 13, and 20 mol % of iron (samples Fe5, Fe13 and

Fe20, respectively). The samples were synthesized in a CO/CO₂ gas-flowing furnace at 1200 °C and $\log f_{\text{O}_2} = -17.4$. Starting materials for the synthesis were pure MgO and ⁵⁷Fe-enriched Fe₂O₃ powders, which were carefully ground, mixed together, and compressed in dense pellets to provide better intergranular connection. The samples were annealed for ~ 100 hours and during this period twice crashed and regrained in order to achieve good chemical heterogeneity. Samples then were rapidly quenched into cold reservoir with the same gas mixture to prevent possible iron oxidation. Samples purity has been checked with the x-ray diffraction, Mössbauer spectroscopy and microprobe analysis, and no chemical heterogeneities were observed. The Fe³⁺/ Σ Fe ratio was about 3.2% for the Fe20 sample, 2.5% for the Fe13 sample, and 1.5% for the Fe5 sample.

High-pressure Mössbauer spectroscopic measurements were performed using a diamond-anvil-cell (DAC) technique. We used diamond anvils with 250 to 400 μm culet sizes. Final Re gasket thickness was 15 or 30 μm and the sample chamber was 125 to 150 μm in diameter. A constant-acceleration Mössbauer spectrometer with transmission geometry was equipped with a high-specific activity point ⁵⁷Co source in a Rh matrix. Two types of experiments were done, under purely hydrostatic conditions using an ethanol:methanol:water (16:3:1) mixture as a pressure transmission medium up to 11 GPa, and under nonhydrostatic conditions without pressure medium up to 105 GPa. Small ruby chips were loaded in the DAC together with the sample for the pressure determination.²⁰

The x-ray absorption nears edge structure (XANES) measurements were carried out on the dispersive x-ray absorption beamline ID24 at the ESRF. The gap of the undulator was optimized to have the maximum of the first harmonic in the energy range 7000–7500 eV. The optics comprised a pair of curved SiC mirrors in a Kirkpatrick Baez geometry at a grazing incidence angle of 3 mrad, followed by a Si(111) polychromator crystal in the Bragg geometry and an additional vertically focusing Si mirror at a grazing incidence of 3.5 mrad.²¹ The size of the beam on the sample was approximately 10 $\mu\text{m} \times 10 \mu\text{m}$ full width at half maximum (FWHM). Spectra were recorded using a charge-coupled-device (CCD)-based position sensitive detector in the energy range 7070–7330 eV for Fe K-edge. Pixel-energy calibration was obtained by measuring spectra on a reference Fe foil sample.

The *ab initio* calculations were performed within the generalized gradient approximation (GGA) of the density-functional theory (DFT). We used the frozen-core all electron projector augmented wave (PAW) method, as implemented in the *ab initio* total-energy and molecular-dynamics program Vienna *ab initio* simulation program (VASP).²² We used the GGA+*U* formalism formulated by Dudarev *et al.*¹⁰ to account for the strong on-site Coulomb repulsion among rather localized *d* electrons of iron. In this approach only the difference between *U* and *J* is significant,¹⁰ and consequently we will henceforth treat them as one single parameter, for simplicity labeled as *U*.

For the supercell calculations we used either a $4 \times 4 \times 4$ Monkhorst-Pack *k* point mesh²³ (two irreducible *k* points) and Gaussian smearing with a smearing parameter of 0.20

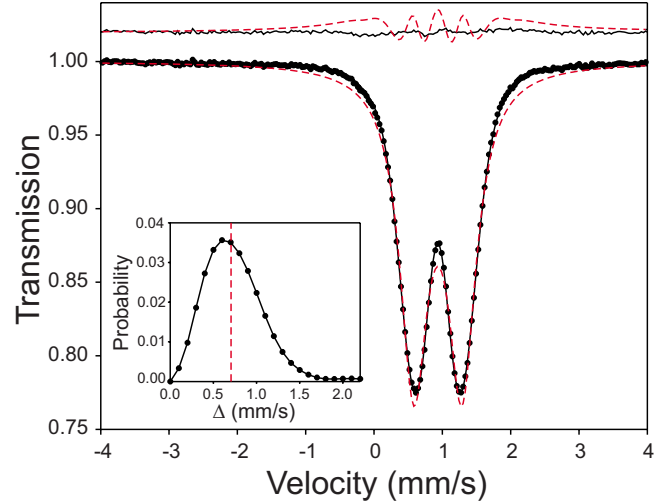


FIG. 1. (Color online) Mössbauer spectrum at ambient conditions of the Fe20 sample (circles), simulated Lorentzian line-shape spectrum (dashed line), and quadrupole splitting distribution (QSD) model (solid line). Residuals for both models are shown above the spectrum. The doppler velocity is given relative to the ⁵⁷Co:Rh source. Inset: quadrupole splitting distribution function. The dashed line shows the QS value from the Lorentzian line-shape analysis.

eV. To assure accurate results we used a plane-wave cutoff energy of 600 eV for all calculations. We modeled (Mg,Fe)O using a $2 \times 2 \times 2$ supercell (64 atom sites), derived from the ideal NaCl structure. Different concentrations of iron were modeled by changing the number of iron atoms in the supercell. For the chosen supercell changing one Mg for a Fe atom would correspond to the concentration of 3.125% Fe. For the Fe atom eight electrons were treated as valent. Our test calculations showed that the inclusion of the semicore Fe *p* states into calculation did not noticeably change results in the considered pressure range considered here.

III. AMBIENT-PRESSURE RESULTS AND THE ANALYSIS OF MÖSSBAUER SPECTRA

Mössbauer spectra of the studied ferropericlase samples at ambient conditions show paramagnetic-type absorption with a well-resolved quadrupole splitting (QS) (indicated by the symbol Δ) (Fig. 1). (Mg,Fe)O is a cubic oxide with a NaCl-type crystal structure, and cations should occupy an octahedral position that has nominally perfect cubic symmetry. In such a case there is no electrical field gradient on the Fe²⁺ nuclei, and therefore there should be no quadrupole splitting in the Mössbauer spectrum of FeO or (Mg,Fe)O.²⁴ Indeed, in pure stoichiometric FeO (Ref. 25) or in extremely diluted (Mg,Fe)O,²⁶ where the local cation environment of the Fe ion is extremely homogeneous [all neighbors are Fe in the case of FeO and Mg in the case of highly diluted (Mg,Fe)O], quadrupole splitting is quite small (< 0.2 mm/s). This non-zero value arises from a small Jahn-Teller distortion of the FeO₆ octahedron. In all other cases (Mg,Fe)O Mössbauer spectra show a well-resolved quadrupole splitting,^{17,27} indicating some local distortion of the FeO₆ octahedron.²⁴ This distortion is caused by the nonequivalent next-nearest-

neighbor coordination, and therefore the analysis of quadrupole splitting in ferropericlyase provides information on the local environment of Fe ions.

Experimental Mössbauer spectra could not be described sufficiently well with simple Lorentzian lines, as shown by the dashed line in Fig. 1. This effect is well known for some disordered Fe alloys and implies a distribution of hyperfine parameters. This method was successfully applied to the analysis of hyperfine magnetic splitting²⁸ and quadrupole splitting.²⁹ In particular, Mössbauer spectra of ferropericlyase can be described with a quadrupole splitting distribution model. In such a model a probability distribution of QS can be extracted from the experimental spectra (Fig. 1, inset).

The extraction (or reconstruction) of the quadrupole splitting probability distribution function requires an accurate determination of the experimental absorption peak profile. The theoretical narrow limit for absorption is a Lorentzian peak shape with line width of 0.194 mm/s, which is the natural linewidth of ⁵⁷Fe for the Mössbauer transition. Experimentally absorption peaks are observed to be significantly broader, and can be modeled using a Voigt function. The main contributions to the experimental linewidth and shape are: the natural line width, which is a physical constant, broadening due to multiple absorption in the sample (sample thickness effect), broadening due to source aging (in this study a high-specific activity Mössbauer source was used, and this effect is significant), and the experimental instrumental resolution. The Mössbauer sample thickness effect can be calculated from the known sample composition, ⁵⁷Fe concentration, density, and thickness, while the effect of the emission profile and experimental resolution was determined by measuring a standard material spectrum (iron foil). The isomer shift δ was refined simultaneously with the Δ probability distribution function. Mössbauer spectra of ferropericlyase with different compositions show similar isomer shift (around 1.04 mm/s), while quadrupole splitting varies significantly. Therefore, we assumed no correlation between δ and Δ in the distribution model. All of the Mössbauer spectra analysis and least-squares fitting was performed using NORMOS-90 software.³⁰

In the face-centered cubic (fcc) lattice of ferropericlyase every Fe ion has 12 next-nearest cation neighbors (NNN). We assume that in the case where NNNs are of the same type (12 Mg or 12 Fe), there is no distortion of the central site and the minimum quadrupole splitting should be observed. In the case that one NNN differs from the others (11 Mg+1 Fe or 11 Fe+1 Mg), some small distortion of the central octahedron occurs and Δ is slightly higher, and so on up to the 6 Mg+6 Fe configuration which has the highest Δ . The probability of any configuration can be easily calculated from the known pair-correlation function P_{FeFe} (i.e., the probability of finding an Fe ion in the NNN coordination shell of another Fe ion),

$$P(n) = P_{\text{FeFe}}^n [(1 - P_{\text{FeFe}})^{12-n}] \frac{12!}{n! (12-n)!}, \quad (1)$$

where $P(n)$ is the probability of an Fe ion to have n Fe ions in its NNN coordination shell. In the case of random cation

distribution P_{FeFe} is equal to the Fe concentration $x(\text{Fe})$, while in the case of clusterization $P_{\text{FeFe}} > x(\text{Fe})$. It is usually assumed¹⁷ that in the case of long-range-ordered distributions $P_{\text{FeFe}} < x(\text{Fe})$; however, this is not necessarily true and superstructural cation arrangements should be described by more than one pair-correlation function (not only in the first coordination shell, but also in the second, the third and so on). For disordered and clusterized solutions the consideration of only the first cation coordination shell (NNN) is sufficient and the short-range order parameter σ is given simply by

$$\sigma = \frac{P_{\text{FeFe}} - x(\text{Fe})}{1 - x(\text{Fe})}, \quad (2)$$

where in this notation σ is synonymous with the Warren-Cowley short-range order parameter.³¹ From Eq. (2) it is obvious that $\sigma=0$ for the random (disordered) solution and $\sigma>0$ in case of clusterization (and $\sigma=1$ in the case of complete decomposition of the solid solution into pure MgO and FeO).

The correlation between the local environment of the Fe ion and its quadrupole splitting is not trivial. We found, however, that even the simplest assumptions work relatively well. We assume a linear relationship between quadrupole splitting Δ and the number of nonequivalent NNN cations as

$$\Delta = aN + b, \quad (3)$$

where N is an integer varying between 0 and 6, indicating the number of nonequivalent NNN cations (e.g., $N=3$ for the 3 Fe+9 Mg and 3 Mg+9 Fe configurations), and a and b are fit parameters. In order to obtain the a and b coefficients, one should fit the experimentally observed Δ distribution to the histogram calculated from Eq. (1) assuming a certain P_{FeFe} value. It is known that ferropericlyase samples quenched from high temperatures at ambient pressure are random solutions,¹⁷ and P_{FeFe} therefore is equal to the Fe concentration. We used Δ distribution functions of the Fe20 sample, which has the broader Δ distribution, to calibrate a and b (Fig. 2), and obtained $a=0.233$ mm/s and $b=0.236$ mm/s. Note that the value $\Delta=0.236$ mm/s for the homogeneously surrounded Fe ion obtained here is quite close to the value of ~ 0.19 mm/s obtained by Waychunas *et al.*¹⁷ using a quite different analysis method. After the a and b coefficients are determined, the inverse procedure could be applied to the experimentally observed QS distribution in order to obtain P_{FeFe} and the short-range order parameter σ . With these empirically obtained a and b parameters we calculated the P_{FeFe} values for the synthesized Fe5 and Fe13 samples to be 0.08 and 0.18, respectively, which are reasonably close to the nominal values of 0.05 and 0.13 for the disordered solutions.

Mössbauer hyperfine parameters can also be calculated using *ab initio* methods. The detailed results of our calculations are discussed below, but here it is useful to compare the experimental ambient conditions results with theoretical predictions. The relationship between s -electron charge density and isomer shift is given by

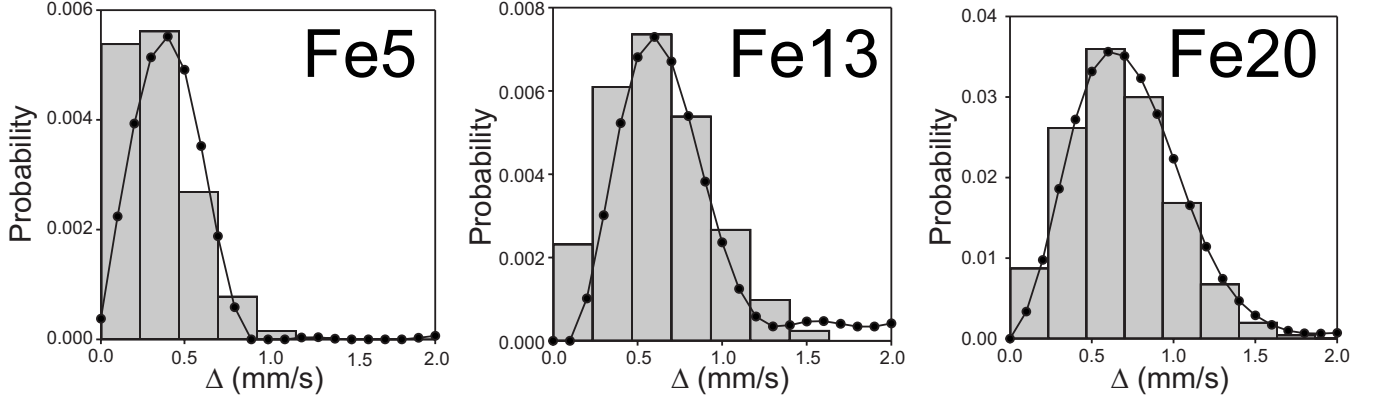


FIG. 2. Quadrupole splitting distribution functions (solid line with black circles) of the samples (from left to right) Fe5, Fe13, and Fe20. Histograms show the simulated distribution according to Eq. (3) (for $P_{\text{FeFe}}=0.08, 0.18$ and 0.20 , from left to right).

$$\delta = \frac{2}{3} \pi Z e^2 \{ |\psi_s(0)_E|^2 - |\psi_s(0)_A|^2 \} \{ \langle R_e^2 \rangle - \langle R_g^2 \rangle \}, \quad (4)$$

where $\langle R_g^2 \rangle$ and $\langle R_e^2 \rangle$ are the mean-square radii of the ground and excited nuclear states, $|\psi_s(0)_E|^2$ and $|\psi_s(0)_A|^2$ are the electron densities at the emitting and absorbing nuclei and Z is the atomic number.³² The mean-square radii of the excited nuclear state could not be calculated or measured directly, and for practical usage a simple relationship $\Delta\delta = \alpha \times \Delta\psi$ is used, where $\Delta\delta$ is the change in isomer shift and $\Delta\psi$ is the change in electron density. Experimental estimation of the coefficient α is straightforward: the electron density for several Fe compounds can be calculated using *ab initio* methods, and isomer shifts can be measured experimentally. However the value of α can vary depending on which theoretical method and compounds are used: literature values vary from -0.11 to $-0.62 \text{ bohr}^3 e^{-1} \text{ sec}^{-1} \text{ mm}$ (Table I). Our approach was to calculate the electron charge density on Fe nuclei in

TABLE I. Conversion parameter α for ^{57}Fe determined by different authors.

α ($\text{bohr}^3 e^{-1} \text{ sec}^{-1} \text{ mm}$)	Author(s)	Year
-0.11	Simanek and Sroubek (Ref. 33)	1967
-0.13	Pleiter and Kolk (Ref. 34)	1971
-0.15	Simanek and Wong (Ref. 35)	1968
-0.15	Sharma and Sharma (Ref. 36)	1972
-0.17	Kündig (Ref. 37)	1976
-0.19	Wakoh and Yamashita (Ref. 38)	1968
-0.23	Duff (Ref. 39)	1974
-0.28	Moyzis and Drickamer (Ref. 40)	1968
-0.33	McNab <i>et al.</i> (Ref. 41)	1971
-0.34	Trautwein <i>et al.</i> (Ref. 42)	1973
-0.37	Ingalls (Ref. 43)	1967
-0.38	Walch and Ellis (Ref. 44)	1973
-0.51	Walker <i>et al.</i> (Ref. 45)	1961
-0.62	Uher and Sorensen (Ref. 46)	1966
-0.32	Present work	

the supercell containing one, two, and three Fe ions for pressures close to ambient, and the resulting values for different numbers of Fe ions were similar. We also calculated the charge density for $\alpha\text{-Fe}$ since experimental values of the center shift reported here are given relative to $\alpha\text{-Fe}$. Only the $\alpha\text{-Fe}$ value and one ferropentacycline calculation at zero pressure were used to calibrate the α coefficient. The value obtained ($-0.32 \text{ bohr}^3 e^{-1} \text{ sec}^{-1} \text{ mm}$) agrees well with many previous determinations (see Table I), suggesting that charge density is predicted accurately using this method.

Mössbauer quadrupole splitting depends on the electrical field gradient (EFG) at the Fe nucleus. The EFG can be described by three principal components: V_{zz} , V_{yy} , and V_{xx} . The eigenvalues of V_{zz} , V_{yy} , and V_{xx} axes are chosen in order of decreasing absolute EFG magnitude, and the direction associated with V_{zz} is called the principal direction of the EFG. The eigenvectors can be averaged according to the scheme

$$V^* = |V_{zz}| \sqrt{1 + \frac{\eta^2}{3}}, \quad (5)$$

with the asymmetry parameter $\eta = \frac{V_{xx} - V_{yy}}{V_{zz}}$.

The quadrupole splitting Δ is given as

$$\Delta = \frac{1}{2} e^2 Q V^*, \quad (6)$$

where Q is the nuclear quadrupole moment of the first-excited state of the absorber nucleus.²⁴ For the ^{57}Fe isotope $Q=0.16 \text{ barn}$.⁴⁷ In the case where the EFG is given in atomic units (au), simply multiplying the EFG by 1.62 gives Δ in units of mm/s. In SI units, the EFG is given in units of V/m^2 , where the conversion factor is $1 \text{ au}=9.7174 \times 10^{21} \text{ V}/\text{m}^2$.

For an isolated Fe ion in a MgO matrix at zero pressure we calculated $\Delta=1.35 \text{ mm/s}$. This value is significantly higher than is expected from our experimental measurements at room temperature (about 0.24 mm/s). This difference can be partially explained by the temperature effect because calculations were carried out for static conditions ($T=0 \text{ K}$). To estimate the temperature effect on the quadrupole splitting, we performed low-temperature Mössbauer spectroscopic measurements of the Fe5 and Fe20 samples down to 80 K .

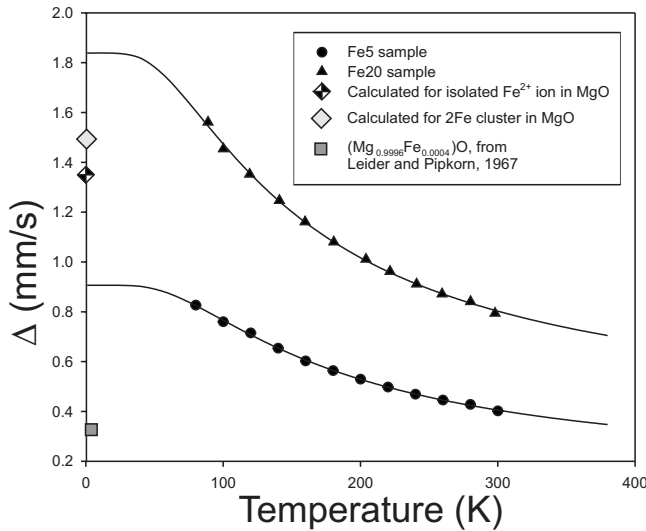


FIG. 3. Temperature dependence of the average quadrupole splitting of the Fe5 and Fe20 samples. Solid lines show the fit to the crystal-field model (Ref. 48). Diamonds show the calculated Δ value for $T=0$ K for an isolated Fe^{2+} and a 2Fe cluster substituting in a MgO matrix. The square shows the experimental value measured at 14 K for $(\text{Mg}_{0.9996}\text{Fe}_{0.0004})\text{O}$ (Ref. 26).

The calculated Δ falls in between the values of these two samples, extrapolated to zero temperature (Fig. 3). Even in the Fe5 sample there is a significant amount of nonisolated Fe ions that increases the quadrupole splitting compared to that for an isolated Fe ion. This implies that the GGA+ U calculations used in this study overestimate the Jahn-Teller effect for the Fe^{2+} ion, and EFG calculations can be evaluated only semiquantitatively.

IV. HIGH-PRESSURE RESULTS: CLUSTERIZATION OF IRON IONS

Upon compression (Mg,Fe)O Mössbauer spectra show unusual behavior. In the relatively low-pressure region (up to 2–3 GPa) the mean QS significantly increases and then continues to slowly increase in a “plateau” region (Fig. 4). This effect was observed in both hydrostatic and nonhydrostatic experiments, and in the latter case QS increases more rapidly. The changes in QS are more pronounced in the Fe5 sample. On decompression Δ decreases but does not return to its initial value, and Mössbauer spectra of the samples quenched from high pressure differ significantly from those quenched from the high-temperature–ambient-pressure synthesis. This observation has several important implications. Different short-range order states of the same material can be quenched to ambient conditions, but only one state can be thermodynamically stable. This means that interatomic diffusion at ambient temperature is extremely slow and the SRO achieved at high P or high T is kinetically frozen. In order to establish a particular short-range order Fe and Mg ions must move between octahedral positions in the oxygen close-packed network. We have no direct information on this mechanism, but it is enhanced dramatically during compression. As normal diffusion kinetics is virtually frozen at room

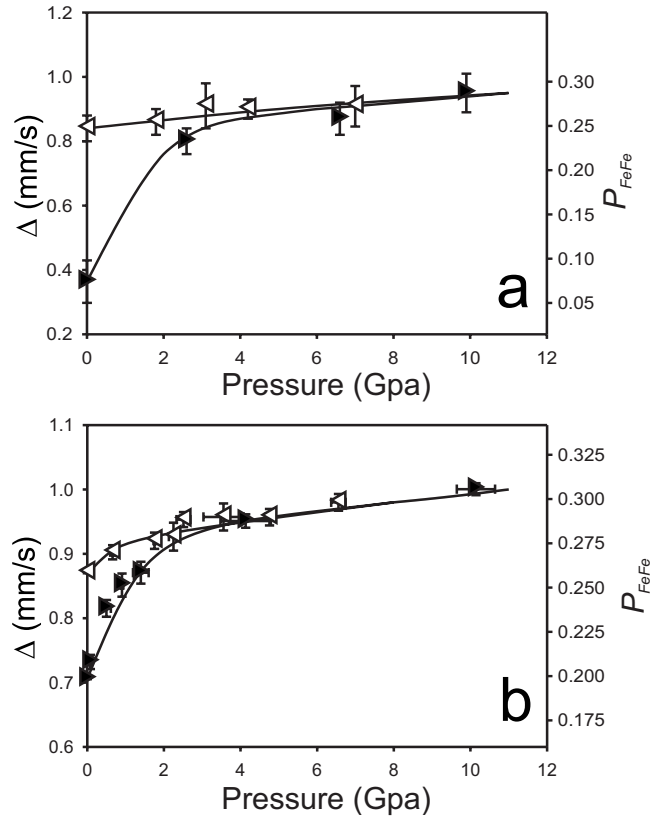


FIG. 4. Pressure dependence of the quadrupole splitting of the Fe5 and Fe20 samples (a and b, respectively). Black triangles pointing to the right are compression points, while white triangles pointing to the left are decompression points. Lines are given as a guide for the eye.

temperature, there are other sources of energy required to overcome the kinetic barrier. The compression itself transfers a significant amount of energy into the system. For instance, if MgO is compressed adiabatically to 10 GPa, it would heat up by several hundred degrees. During static compression this energy is normally dissipated, but it might be partly absorbed for the processes discussed. Another and potentially more important energy source is the mechanical intergranular friction due to deformation of a polycrystalline aggregate. If the latter process is the dominant source of energy, one might predict that a (Mg,Fe)O single crystal would show much more subtle SRO changes during isothermal compression in a hydrostatic pressure medium.

A second important observation is that the SRO is significant under high pressure, and Fe ions form local clusters. This agrees with the observed decomposition of ferroperrichase under high pressure and temperature.^{18,19} Fe cluster formation could also significantly affect many physical properties of the solid solution, especially those related to Fe electronic properties (magnetic and spin state). In particular, the local environment of Fe^{2+} (and, therefore, Fe-Fe exchange and superexchange interactions) in the Fe5 sample under pressure is very similar to that in the randomly distributed Fe20 composition.

High temperature favors a disordered cation distribution mainly due to the entropy contribution. Entropy is, in prin-

principle, a function of short-range order. Excess SRO entropy consists of two main components: configurational and excess vibrational entropies. Excess vibrational entropy could be either positive or negative, and its evaluation is not straightforward. In contrast, configurational entropy can be easily estimated, and for the fcc cation lattice with only first-term (NNN) correlations can be written as follows:⁴⁹

$$\Delta S_{conf} = -3k_B\sigma^2, \quad (7)$$

where k_B is the Boltzmann constant and σ is the SRO parameter. In our experiment we found that SRO is higher in low-Fe samples, and is maximum for the Fe5 sample. Under high pressure the pair-correlation function P_{FeFe} is about 0.28 and the corresponding σ value is 0.242 (Fig. 4). Therefore, at room temperature the $-T\Delta S_{conf}$ contribution to the Gibbs free energy (compared to the random cation distribution) is about 0.44 kJ/mol.

The vibrational entropy contribution as a function of SRO is not known. The vibrational entropy difference between completely decomposed ($\sigma=1$) and completely disordered ($\sigma=0$) solutions is given as⁵⁰

$$\Delta S_{vibr} = 3k_B \ln\left(\frac{\theta_D}{\theta'_D}\right), \quad (8)$$

where θ_D and θ'_D are the Debye temperatures of the mechanical mixture of the components and of the random solid solution, respectively. The $\frac{\theta_D}{\theta'_D}$ ratio is not lower than 0.93 for Mg-rich ferroperricite,⁵¹ and at room temperature the $-T\Delta S_{vibr}$ contribution does not exceed 0.48 kJ/mol. For $0 < \sigma < 1$ this contribution should be smaller, but it still has the same order of magnitude as the configurational entropy contribution for the Fe5 sample. This implies that the enthalpy gain due to short-range ordering (ΔH_{SRO}) should be of the order of kJ/mol, which is significant. The nature of ΔH_{SRO} is clear: if the energy of the Fe-Mg bond $E_{Fe-Mg} < \frac{1}{2}(E_{Fe-Fe} + E_{Mg-Mg})$, then Fe ions would tend to separate from each other and the solid solution would tend to form an ordered superstructural compound (like in the CuAu alloy⁵²). In the case when $E_{Fe-Mg} \approx \frac{1}{2}(E_{Fe-Fe} + E_{Mg-Mg})$ there is no tendency for ordering, and a disordered random solution is formed due to the entropy contribution. Finally, if $E_{Fe-Mg} > \frac{1}{2}(E_{Fe-Fe} + E_{Mg-Mg})$, then Fe ions would prefer to be surrounded by Fe ions only and the tendency for clusterization and further possible decomposition of the solid solution is developed. According to our experimental observations, the latter case exists at least in the low-Fe part of the (Mg,Fe)O solid solution.

In order to verify this suggestion, we performed *ab initio* calculations of (Mg,Fe)O with various relative Fe arrangements. In the $2 \times 2 \times 2$ supercell that we used in our calculations, there are 32 cation positions. When we replace one Mg with Fe, iron ions are located quite far away from each other and are not interacting. In this case the composition of the supercell corresponds to $(Mg_{0.96875}Fe_{0.03125})O$. All of the symmetrization was switched off in the calculation, allowing ions to shift from their high-symmetry positions. Although the local Fe surrounding is perfectly cubic in this case, the FeO_6 octahedron shows a small Jahn-Teller distortion. Fe-O

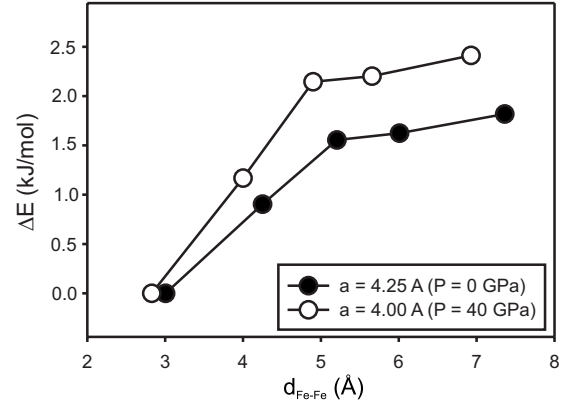


FIG. 5. Calculated enthalpy difference for the $(Fe_2Mg_{30})O_{32}$ supercell as a function of Fe-Fe distance. Black circles are for $a = 4.25$ Å (pressure about 0 GPa) and open circles are for $a = 4.00$ Å (pressure about 40 GPa).

distances are nonequivalent: four oxygen ions are at 2.176 Å from the central Fe and two oxygen ions are at 2.130 Å. This small distortion supports our experimental observation of the small quadrupole splitting produced by Fe ions in a homogenous local surrounding. If we replace another Mg by Fe, the total composition is $(Mg_{0.9375}Fe_{0.0625})O$, fairly close to the Fe5 sample composition. Inside the 32 atom supercell we can place the second Fe ion in the first (NNN position), second, third, fourth, or sixth cation coordination shell. All of these possibilities were tested for two different volumes, with lattice parameter a equal to 4.25 and 4.00 Å, which corresponds to pressures of approximately 0 and 40 GPa, respectively. The calculated energy difference between these configurations is remarkable (Fig. 5). The energy difference is given per one oxygen atom, and absolute values are shifted to produce a zero value for the configuration with two Fe ions as the closest (NNN) neighbors. The configuration with two Fe forming a pair cluster is much more favorable compared to all other configurations. There is almost no energy difference when the second Fe ion is in at least the third or more distant coordination shells, implying almost no Fe-Fe interactions at a distance of larger than ~ 5 Å. However the second coordination shell is energetically in between the first (NNN) shell and more distant coordination shells. This implies that for an accurate description of the (Mg,Fe)O solid solution [for example, within the cluster-variation method CVM (Ref. 53)], at least the second correlation function need to be included in the model. The second conclusion that can be drawn directly from Fig. 5 is that increasing pressure increases ΔH_{SRO} : when going from 0 to 40 GPa, the energy difference between NNN and noninteracting configurations increases by $\sim 30\%$.

The results of our calculations are not sufficient to treat them formally using the CVM; however we attempt estimates using a simplified CVM for the highly dilute solid solution. For the 6.25%Fe composition in the random solution more than 80% of Fe ions are either isolated from each other, or form pairs. If we assume that only these two configurations are possible, then a random solution can be de-

scribed as 25% Fe ions that are isolated and 75% Fe ions with another Fe as its NNN. The configuration with all Fe forming NNN pairs would have $P_{\text{FeFe}}=1/12$ and $\sigma=0.0222$. In this case $\Delta H_{\text{SRO}}=-0.36$ kJ/mol from our calculations, and at room temperature $-T(\Delta S_{\text{conf}}+\Delta S_{\text{vibr}})$ is on the order of 0.1 kJ/mol. In other words the enthalpy effect dominates over the entropy contribution and equilibrium SRO could be even higher, implying the formation of a significant number of multiatomic (more than three atoms) Fe clusters in the solid solution. This estimate strongly supports our experimental observations concerning the significant SRO, especially for low-Fe concentrations in the (Mg,Fe)O solid solution.

Another interesting result of our experimental study is that changes of short-range order are much higher for the Fe5 sample compared to the Fe20 sample (see Fig. 4). In the Fe5 sample before compression the maximum probability corresponds to the two-atom 2Fe cluster. After compression, the three-atom 3Fe cluster is the most common. We infer that the 3Fe cluster is energetically the most stable, and dilute Fe ions tend to form 3Fe clusters. The most probable configuration of the 3Fe cluster is a Fe triangle in the $\langle 111 \rangle$ plane (inside a closed-packed layer of cations), in which every Fe ion has two NNNs (for comparison, in a 3Fe linear chain only the central ion has two NNNs). In the Fe20 sample in the random solution already most of the Fe ions are in 3Fe clusters; therefore changes in the SRO are much smaller. The enthalpy gain of clusters formed by four and higher numbers of Fe atoms is probably much smaller, and the enthalpy penalty suppresses strong SRO in compositions with higher Fe content.

Additional experimental constraints beyond simplified thermodynamic estimates are necessary to fully understand the P and T limits for significant SRO in (Mg,Fe)O. The only reasonable approach is to equilibrate (Mg,Fe)O samples at different conditions and to compare the quadrupole splitting distribution of the quenched samples. Three experiments with the Fe20 sample were performed: compression at room temperature up to 30 GPa; annealing in the multianvil large-volume press at 18 GPa and 1000 °C; and a laser-heating experiment in the diamond-anvil cell at 40 GPa and ~ 1800 °C. The latter two spectra were taken from McCammon *et al.*⁵⁴ In the laser-heating experiment the temperature was not measured, so the value of 1800 °C is a rough estimation. The resulting quadrupole splitting distributions are shown in Fig. 6. The starting material (annealed at ambient pressure and 1200 °C) and the sample annealed at 18 GPa and 1000 °C show very similar Mössbauer spectra which are assigned to the (almost fully) disordered cation distribution. In contrast, the sample at 40 GPa (laser heated) is almost identical to those treated at room temperature and 30 GPa. This implies that significant SRO should exist at mantle conditions since pressure strongly stabilizes clusterization in ferropentacycline.

Additional evidence for the changes in short-range order is provided by XANES spectroscopy, which is a local probe and has chemical sensitivity. In principle, a complete understanding of the local geometry and site coordination around Fe can be obtained from XANES. However, the quantitative analysis of this region presents difficulties mainly related to

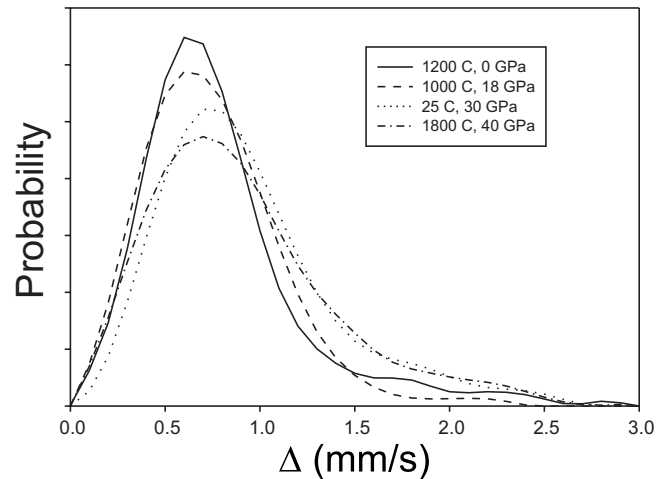


FIG. 6. Quadrupole splitting distribution of Fe20 samples with different P and T histories. Solid line—starting material, equilibrated at 1200 °C and ambient pressure. Dashed line—sample, annealed at 1000 °C and 18 GPa in a large-volume multianvil press. Dotted line—sample after compression to about 30 GPa at room temperature. Dashed-dotted line—laser-heated sample (approximately 1800 °C) at 40 GPa.

the theoretical approximation in the treatment of the potential and the need for heavy time-consuming algorithms to calculate the absorption cross section in the framework of a full multiple-scattering approach. In order to verify the sensitivity of XANES to compositional variations in the NNN shell we have performed a comparison of the data with full multiple-scattering calculations using a self-consistent energy-dependent exchange-correlation Hedin-Lundqvist potential (FEFF8 package⁵⁵). Self-consistency was obtained by successively calculating the electron density of states, electron density, and Fermi level at each stage of the calculation within a 33-atom cluster (corresponding to four neighbor shells) centered on the atom for which the density of states is calculated, and then iterated. Full multiple-scattering XANES calculations were carried out for this cluster: all multiple-scattering paths within this cluster were summed to infinite order. Besides the structural information defining the geometry of the cluster [we simulated a $(\text{Mg}_{0.90}\text{Fe}_{0.10})\text{O}$ cluster with $a=4.225$ Å], no other external parameters were used as input for the XANES simulations, except for a -2 eV shift of the energy axis. The results of the three simulations are shown in Fig. 7(a), where we plot the case of zero, six, and 12 Fe atoms as NNN. We can clearly see that chemical ordering modifies significantly the energy region of the inflection point at ~ 7123 eV, which becomes smaller with increasing Fe content in the NNN shell, and completely disappears for the case of 12 NNN (all Fe).

Figure 7(b) shows experimental XANES spectra of the Fe5, Fe13, and Fe20 samples recovered after compression in DACs to over 20 GPa, the spectrum of the Fe13 starting material as well as that of pure wüstite ($\text{Fe}_{0.94}\text{O}$). There are clear composition-dependent changes in the edge structure of (Mg,Fe)O solid solutions. The inflection point at ~ 7123 eV becomes smaller with increasing Fe content, and completely disappears in the $\text{Fe}_{0.94}\text{O}$ XANES spectrum, in good agree-

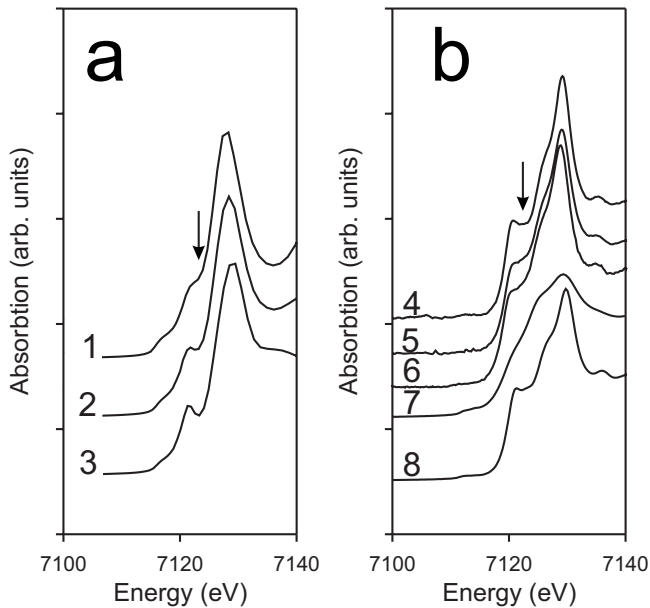


FIG. 7. Fe K -edge XANES spectra in the MgO-FeO system. (a) Full multiple-scattering simulations of $(\text{Mg}_{0.90}\text{Fe}_{0.10})\text{O}$ with $a = 4.225 \text{ \AA}$ where we have modified the chemical composition of the NNN shell. Spectra 1 to 3 are for 12, six, and zero Fe atoms in the NNN shell of the absorbing atom, correspondingly. (b) Experimentally measured XANES spectra. Spectrum 4 is the Fe5 sample after compression; 5—Fe13 sample after compression; 6—Fe20 sample after compression; 7—FeO wüstite sample. 8—Fe13 starting material. The arrow indicates the region of major changes in the XANES spectra due to changes in local Fe coordination.

ment with the multiple-scattering simulations.

There is a clear difference in the XANES spectrum of the Fe13 sample before and after compression [curves 5 and 8 in Fig. 7(b)]. The local Fe concentrations in the Fe13 and Fe20 samples after compression are almost identical. The Fe5 sample after compression shows a XANES spectrum almost identical to that of the Fe13 sample before compression (curves 4 and 8), which implies more than a twofold increase in local Fe concentration around the Fe atom, in full agreement with the Mössbauer data.

V. LOCAL COORDINATION AND SPIN STATE

Spin crossover [transition from the high-spin (HS) state with four unpaired d electrons to the low-spin (LS) state with all d electrons paired] of Fe^{2+} in $(\text{Mg},\text{Fe})\text{O}$ under high pressure has been the subject of a large number of studies in the past few years.¹⁻⁵ Although there is general agreement that the transition occurs and affects $(\text{Mg},\text{Fe})\text{O}$ density and elasticity, the details of spin crossover and its pressure, temperature, and compositional dependence remain unclear.

Room-temperature Mössbauer spectra of $(\text{Mg},\text{Fe})\text{O}$ samples with different compositions were collected up to 105 GPa, and at high pressure clear changes were observed, consistent with spin crossover. Above ~ 50 GPa a new component appears in the Mössbauer spectra of all studied ferropericlases. This new component has virtually zero quadrupole splitting and an isomer shift somewhat smaller

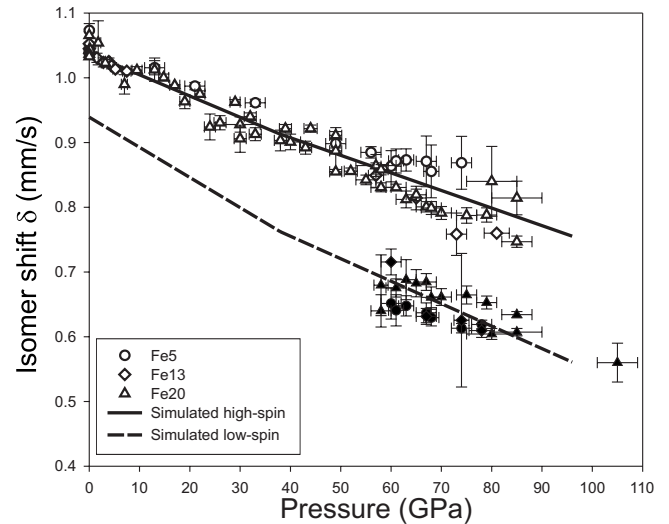


FIG. 8. Pressure dependence of $(\text{Mg},\text{Fe})\text{O}$ isomer shift (relative to $\alpha\text{-Fe}$). Open and closed symbols are for high- and low-spin components, respectively. Circles, diamonds, and triangles are for Fe5, Fe13, and Fe20 samples, respectively. Solid and dashed lines show the results of *ab initio* simulations.

than the high-spin component. This is typical for low-spin Fe^{2+} : when there are no unpaired electrons, the charge distribution becomes significantly more symmetrical and the EFG becomes essentially zero because of the disappearance of the valence electron EFG contribution. The total charge (electron) density at the Fe nucleus increases, and this is the reason for the IS decrease. The absolute change of the isomer shift (Fig. 8) is, however, relatively small ($\sim 0.17 \text{ mm/s}$) compared to those usually observed for iron-organic complexes ($\sim 0.5 \text{ mm/s}$).⁵⁶ However, this small difference between high- and low-spin Fe^{2+} atoms in $(\text{Mg},\text{Fe})\text{O}$ is fully consistent with our *ab initio* simulations, shown in Fig. 8. There was no significant difference in charge density for the isolated Fe ion, and for 2Fe and 3Fe clusters. Calculations were made for the cell parameter $a = 4.25, 4.00, \text{ and } 3.80 \text{ \AA}$ and for high- and low-spin iron electronic configurations. The isomer shift was found to be nearly independent of the local Fe surrounding, similar to what is observed in experiments.

On compression at ambient temperature, in all three ferropericlase samples (Fe5, Fe13, and Fe20) the low-spin component gradually increases with pressure, and the amount of the high-spin component decreases accordingly (Fig. 9). The high-spin and low-spin fractions were calculated from the absorption areas of the subspectral components, assuming equal Debye-Waller factors of the HS and LS Fe ions. While this is not exactly true, this difference is small and can usually be neglected.⁵⁶ The samples studied were highly enriched with ^{57}Fe and the effective Mössbauer thickness was much higher than for a “thin” absorber. The high thickness of the absorber causes significant internal multiple absorption, which can markedly distort the relative areas of the two subspectral components in the mixed spin region. To avoid these effects we applied thickness corrections using a full transmission integral calculation.⁵⁷

The range over which high- and low-spin states coexist is remarkable: for the Fe5 sample it is about 30 GPa, and more

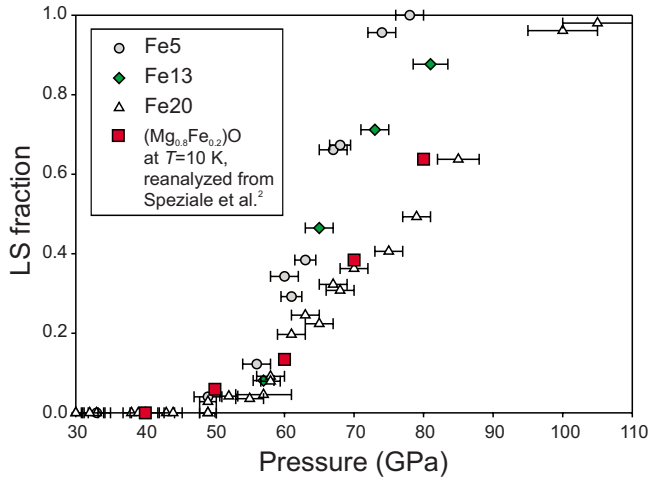


FIG. 9. (Color online) Low-spin fraction in ferroperricite as a function of pressure. Gray circles, green diamonds, and open triangles are for Fe5, Fe13, and Fe20 samples at room temperature, respectively. Red squares—reanalyzed data from Speziale *et al.* (Ref. 2), collected at 10 K for the $(\text{Mg}_{0.8}\text{Fe}_{0.2})\text{O}$ sample. See text for details.

than 50 GPa for the Fe20 sample (Fig. 9). Such a broad region of spin crossover cannot be attributed to pressure gradients in the DAC. With several small ruby chips placed in different parts of the sample chamber, pressure gradients could be measured and were no higher than 5–7 GPa at the highest pressure reached (over 100 GPa).

VI. SPIN CROSSOVER

In order to understand these results on spin crossover in ferroperricite, one should consider the physical nature of these changes. Spin crossover in ferroperricite is often discussed in terms of a phase transition. A number of previous studies focused on determination of the volume (density) collapse and the magnitude of elastic wave velocity discontinuities associated with the spin transition. The question of whether it is a first- or a second-order transition has also been discussed.^{2,58–60} However, spin crossover is not necessarily a phase transition. In order to apply a thermodynamic theory of phase transitions, there should be two distinct phases—a high-spin and a low-spin phase. In the case of two or more possible different states of an atom (in this case high- or low-spin electronic configurations), all the states have always (at any finite temperature) a certain nonzero probability. Every energy level or quantum state of an atom is populated as described by the Boltzmann thermal population function. This means that in any Fe^{2+} compound and under any thermodynamic conditions, there are some iron ions in a high-spin and some in a low-spin state. Usually, one state is dominating and the other state has negligible population, and a compound is considered to be either high or low spin. However, there can be a continuous change in spin probability between these two states. The term “spin crossover” reflects this particular idea: at certain P and T conditions the low-spin and the high-spin probabilities are equal. Different molecules or ions within the same crystal exist in

different spin states while the crystal is still a single phase.⁶¹ When both spin states of iron coexist in significant amounts in a single crystal, they cannot be considered as two distinct phases. However, the physical properties and chemical bonding in high- and low-spin Fe compounds can be significantly different, giving rise to a real phase transition. If, as a result of spin state changes, two different (in a thermodynamic sense; i.e., different Gibbs energies) phases appear, it should be described as a phase transition. For example, in the case of a volume discontinuity or changes in crystal symmetry, spin crossover can be described in terms of a phase transition.

All of our experimental observations are consistent with spin changes in Mg-rich $(\text{Mg},\text{Fe})\text{O}$ at high pressure occurring as spin crossover without phase transition (e.g., we have no evidence of the existence of different regions of the samples, grains, or even domains with distinctly different volume, symmetry, compositions, defined boundaries, etc.), and in this case the high-spin and low-spin populations should follow the Boltzmann distribution

$$\frac{\Lambda_{\text{LS}}}{\Lambda_{\text{HS}}} = \exp\left(-\frac{\Delta H}{k_B T}\right), \quad (9)$$

where Λ_{LS} and Λ_{HS} are relative fractions of low- and high-spin molecules (atoms) in the crystal, ΔH is the enthalpy difference between the high- and low-spin states, k_B is the Boltzmann constant, and T is the absolute temperature. ΔH is a function of thermodynamic parameters and should change its sign with varying thermodynamic parameters to satisfy spin crossover conditions. When $\Delta H=0$ the populations of high- and low-spin Fe atoms are equal, and this point is called spin crossover. In a pressure-induced spin crossover ΔH changes with pressure at constant temperature, passing through zero at some crossover pressure. Usually the enthalpy difference between two phases or electronic states—here ΔH —changes almost linearly with pressure, at least in the vicinity of the critical pressure. Our *ab initio* calculations also support this hypothesis as shown below. The character of spin crossover (i.e., its broadness) therefore depends on temperature and the pressure dependences of ΔH . The latter should not change significantly with temperature, and only the crossover pressure should be temperature dependent.

Low-temperature measurements can give additional important information concerning the physical properties of spin crossover. Low-temperature Mössbauer spectra at 10 K for $(\text{Mg}_{0.8}\text{Fe}_{0.2})\text{O}$ were collected up to 80 GPa by Speziale *et al.*² A reanalysis of the original data² based on a two-component fitting of each spectrum shows a significant amount of the high-spin component even at the highest pressure. The width and pressure of spin crossover at 10 K is virtually the same as at 300 K (Fig. 9). This fact implies that the spin crossover for the Fe20 sample cannot be described with Eq. (9) because temperature strongly affects the Boltzmann distribution. However, if the spin transition occurs in several steps, the total width of the transition zone would be much less broadened by temperature: there would be either several sharp steps at low temperature or several broad steps at high temperature. If there are different types of Fe ions in the crystal, they could have different critical crossover pres-

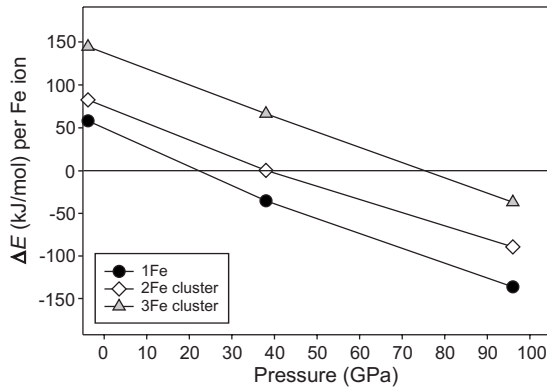


FIG. 10. Calculated energy difference between the high- and low-spin states of Fe in different Fe clusters.

tures. Such a behavior (steplike spin transition) is known for many metal-organic complexes, for example $[\text{Fe}(\text{2-pic})_3]\text{Cl}_2 \times \text{EtOH}$.⁶²

The reason for different Fe^{2+} ions to have different crossover pressures is the difference in the local environment. An isolated Fe^{2+} ion readily transforms to the low-spin state. When another Fe ion is placed in the first coordination shell, a significant electronic exchange between Fe ions appears. This electronic exchange stabilizes the high-spin state relative to the low-spin state. This idea is supported by static *ab initio* calculations (Fig. 10). The critical pressure is different for different Fe clusters: it is about 20 GPa for the isolated Fe ion, while for a 2Fe cluster it is about 40 GPa.

The pressure dependence of ΔE remains virtually the same. Based on these static ($T=0$) *ab initio* results, one can calculate the temperature effect using Eq. (9). If we consider a hypothetical $(\text{Mg,Fe})\text{O}$ solid solution with 29% of Fe ions being isolated, 38% forming pairs, and 33% forming 3Fe clusters, we can calculate spin crossover for different pressures and temperatures (Fig. 11). This cluster distribution is close to those for $P_{\text{FeFe}}=0.1$, with all clusters larger than 3Fe neglected.

The height of each step of the spin transition depends on the relative abundance of different Fe clusters. Different cluster abundances are defined by the composition and short-range order. Separation (pressure difference) between these steps is controlled by the strength of electronic exchange between neighboring Fe ions. Electronic exchange interactions normally decrease with increasing temperature.^{63,64} The total fraction of low-spin Fe^{2+} ions depends therefore not only on pressure, temperature, and composition, but also on short-range order, a phenomenon that is often ignored in solid solutions.

The temperature effect on spin crossover requires additional consideration. A “normal” temperature effect shifts the critical point to higher pressures. This is the effect of thermal expansion combined with a higher entropy contribution (the electronic entropy of the high-spin state is higher than that of the low-spin state). Temperature also increases the width of the transition region according to Boltzmann statistics, so the “beginning” of the transition would occur at lower pressures and “completion” of the transition would shift to higher pressures. The decrease in exchange interactions gives a different

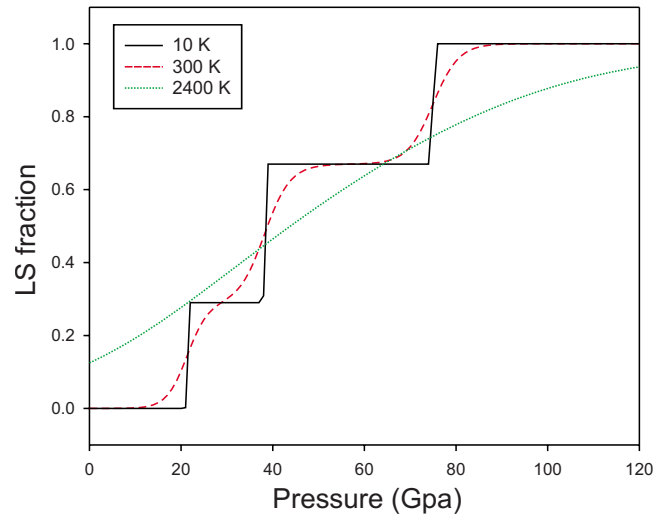


FIG. 11. (Color online) Low-spin fraction at different temperatures from *ab initio* calculations (see text for details). Solid black line is for 10K, dashed (red) line is for 300K and dotted (green) line is for 2400K. Only the temperature contribution to Boltzmann statistics was taken into account.

effect: the width of different steps decreases, and the critical pressure for different Fe clusters approaches that of an isolated Fe ion. As a result, the total transition width could even decrease from the high-pressure side with increasing temperature. The temperature effect on spin crossover in ferropericlase contains several competing contributions, and if they completely cancel each other, temperature could have no effect on the total spin crossover in ferropericlase.

Several high-temperature Mössbauer spectroscopic measurements were performed for the Fe5 and Fe20 samples up to 750 K using a resistively heated DAC. The observed temperature dependence of the spin crossover is remarkable: for the Fe20 sample almost no temperature effect on crossover pressure and transition width was observed [Fig. 12(b)]. For the Fe5 sample increasing temperature results in a slight decrease in the crossover pressure, while the transition width remains virtually the same [Fig. 12(a)]. These features can be explained only within the steplike spin crossover model with each step following Boltzmann statistics, as described above.

In terms of applications to the earth’s lower mantle, high temperature (2000–2400 K) would cause the spin transition in ferropericlase to be very broad and to occur over the entire

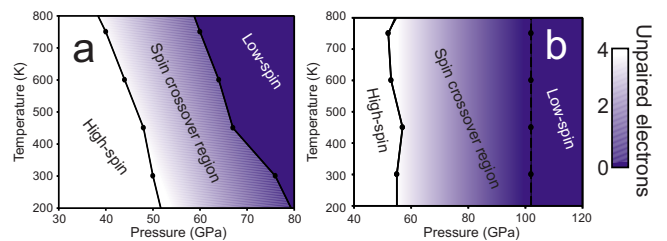


FIG. 12. (Color online) Temperature dependence of spin crossover in Fe5 (a) and Fe20 (b) ferropericlase samples, measured using the Mössbauer spectroscopy in resistively externally heated DAC. Boundaries are drawn at the point where low-spin or high-spin states are no longer detectable.

depth range of the mantle, as also suggested by other studies.^{59,60} Even if electronic exchange interactions completely disappeared at these temperatures and the transition occurred in a single step, the broadness of the transition at these temperatures would be significant. Therefore no pronounced discontinuities in any physical property of ferropericlase which depend on spin state are expected at lower mantle conditions. Indeed, no strong seismic wave discontinuities are known in the lower mantle.

VII. CONCLUSIONS

Fe ions in (Mg,Fe)O demonstrate significant changes in short-range order and deviations from regular solid solution. The degree of short-range order changes dramatically with

pressure, and clear signs of Fe ion clusterization were observed and also supported by *ab initio* simulations. Pressure-induced spin crossover in ferropericlase does not show features characteristic for a phase transition. On the contrary, it can be understood as thermally equilibrated high- and low-spin states coexisting in the same phase. The relative population of high- and low-spin Fe²⁺ ions depends not only on pressure, temperature, and composition, but also on the short-range ordering.

ACKNOWLEDGMENTS

We acknowledge the German Science Foundation (DFG) and the European Science Foundation (EuroMinSci project) for financial support of this study.

*Corresponding author; Present address: CARS, University of Chicago, Argonne National Lab, Argonne 60439, USA; kantor@cars.uchicago.edu

- ¹Y. Fei, L. Zhang, A. Corgne, A. Ricolleau, Y. Meng, and V. Prakapenka, *Geophys. Res. Lett.* **34**, L17307 (2007).
- ²S. Speziale, A. Milner, V. E. Lee, S. M. Clark, M. P. Pasternak, and R. Jeanloz, *Proc. Natl. Acad. Sci. U.S.A.* **102**, 17918 (2005).
- ³J. C. Crowhurst, J. M. Brown, A. F. Goncharov, and S. D. Jacobsen, *Science* **319**, 451 (2008).
- ⁴I. Yu. Kantor, L. S. Dubrovinsky, and C. A. McCammon, *Phys. Rev. B* **73**, 100101(R) (2006).
- ⁵H. Keppler, I. Kantor, and L. Dubrovinsky, *Am. Mineral.* **92**, 433 (2007).
- ⁶D. L. Anderson, *New Theory of the Earth* (Cambridge University Press, Cambridge, UK, 2007).
- ⁷C. G. Shull, W. A. Strauser, and O. E. Wollan, *Phys. Rev.* **83**, 333 (1951).
- ⁸Y. Fei and H. K. Mao, *Science* **266**, 1678 (1994).
- ⁹M. P. Pasternak, R. D. Taylor, R. Jeanloz, X. Li, J. H. Nguyen, and C. A. McCammon, *Phys. Rev. Lett.* **79**, 5046 (1997).
- ¹⁰S. L. Dudarev, G. A. Botton, S. Y. Savrasov, C. J. Humphreys, and A. P. Sutton, *Phys. Rev. B* **57**, 1505 (1998).
- ¹¹Z. Fang, I. V. Solovyev, H. Sawada, and K. Terakura, *Phys. Rev. B* **59**, 762 (1999).
- ¹²S. A. Gramsch, R. E. Cohen, and S. Y. Savrasov, *Am. Mineral.* **88**, 257 (2003).
- ¹³A. R. Oganov and P. I. Dorogokupets, *Phys. Rev. B* **67**, 224110 (2003).
- ¹⁴J. M. Cowley, *Phys. Rev.* **77**, 669 (1950).
- ¹⁵M. Morozov, Ch. Brinkmann, W. Lottermoser, G. Tippelt, G. Amthauer, and H. Kroll, *Eur. J. Mineral.* **17**, 495 (2005).
- ¹⁶H. Yang and S. Ghose, *Am. Mineral.* **79**, 633 (1994).
- ¹⁷G. A. Waychunas, W. A. Dollase, and C. R. Ross, II, *Am. Mineral.* **79**, 274 (1994).
- ¹⁸L. S. Dubrovinsky, N. A. Dubrovinskaia, S. K. Saxena, H. Annersten, E. Hälenius, H. Harryson, F. Tutti, S. Rekhii, and T. Le Bihan, *Science* **289**, 430 (2000).
- ¹⁹L. Dubrovinsky, N. Dubrovinskaia, I. Kantor, C. McCammon, W. Crichton, and V. Urusov, *J. Alloys Compd.* **390**, 41 (2005).
- ²⁰H. K. Mao, J. Xu, and P. M. Bell, *J. Geophys. Res.* **91**, 4673 (1986).
- ²¹S. Pascarelli, O. Mathon, and G. Aquilanti, *J. Alloys Compd.* **362**, 33 (2004).
- ²²G. Kresse and J. Furthmüller, *Phys. Rev. B* **54**, 11169 (1996).
- ²³H. J. Monkhorst and J. D. Pack, *Phys. Rev. B* **13**, 5188 (1976).
- ²⁴R. J. Evans, D. G. Rancourt, and M. Grodzinski, *Am. Mineral.* **90**, 187 (2005).
- ²⁵L. Broussard, *J. Phys. Chem.* **73**, 1848 (1969).
- ²⁶H. R. Leider and D. N. Pipkorn, *Phys. Rev.* **165**, 494 (1968).
- ²⁷D. P. Dobson, N. S. Cohen, Q. A. Pankhurst, and J. P. Brodholt, *Am. Mineral.* **83**, 794 (1998).
- ²⁸D. G. Rancourt and J. Y. Ping, *Nucl. Instrum. Methods Phys. Res. B* **58**, 85 (1991).
- ²⁹D. G. Rancourt, *Phys. Chem. Miner.* **21**, 244 (1994).
- ³⁰R. A. Brand, NORMOS-90 Mössbauer Fitting Program Package, Wissenschaftliche Elektronik GmbH, Starnberg, Germany.
- ³¹B. E. Warren, *X-ray Diffraction* (Addison-Wesley, Massachusetts, 1968).
- ³²N. N. Greenwood and T. C. Gibb, *Mössbauer Spectroscopy* (Chapman and Hall, London, 1971).
- ³³E. Šimánek and Z. Šroubek, *Phys. Rev.* **163**, 275 (1967).
- ³⁴F. Pleiter and B. Kolk, *Phys. Lett. B* **34**, 296 (1971).
- ³⁵E. Šimánek and A. Y. C. Wong, *Phys. Rev.* **166**, 348 (1968).
- ³⁶R. R. Sharma and A. K. Sharma, *Phys. Rev. Lett.* **29**, 122 (1972).
- ³⁷W. Kündig, *Hyperfine Interact.* **2**, 113 (1976).
- ³⁸S. Wakoh and J. Yamashita, *J. Phys. Soc. Jpn.* **25**, 1272 (1968).
- ³⁹K. J. Duff, *Phys. Rev. B* **9**, 66 (1974).
- ⁴⁰J. A. Moyzis and H. G. Drickamer, *Phys. Rev.* **171**, 389 (1968).
- ⁴¹T. K. McNab, H. Micklitz, and P. H. Barrett, *Phys. Rev. B* **4**, 3787 (1971).
- ⁴²A. Trautwein, J. R. Regnard, F. E. Harris, and Y. Maeda, *Phys. Rev. B* **7**, 947 (1973).
- ⁴³R. Ingalls, *Phys. Rev.* **155**, 157 (1967).
- ⁴⁴P. F. Walch and D. E. Ellis, *Phys. Rev. B* **7**, 903 (1973).
- ⁴⁵L. R. Walker, G. K. Wertheim, and V. Jaccarino, *Phys. Rev. Lett.* **6**, 98 (1961).
- ⁴⁶R. A. Uher and R. A. Sorensen, *Nucl. Phys.* **86**, 1 (1966).
- ⁴⁷P. Dufek, P. Blaha, and K. Schwarz, *Phys. Rev. Lett.* **75**, 3545

- (1995).
- ⁴⁸S. G. Eekhout, E. De Grave, C. A. McCammon, and R. Vochten, *Am. Mineral.* **85**, 943 (2000).
- ⁴⁹I. Tsatskis, *J. Phys.: Condens. Matter* **10**, L683 (1998).
- ⁵⁰V. S. Urusov, V. L. Tauson, and V. V. Akimov, *Solid State Geochemistry* (GEOS, Moscow, 1997).
- ⁵¹S. D. Jacobsen, H.-J. Reihmann, H. A. Spetzler, S. J. Mackwell, J. R. Smyth, R. A. Angel, and C. A. McCammon, *J. Geophys. Res.* **107**, 2037 (2002).
- ⁵²H. Sato and R. S. Toth, in *Long Period Superlattices in Alloys, in Alloying Behavior and Effects in Concentrated Solid Solutions*, edited by T. B. Massalski (Gordon and Breach, New York, 1965).
- ⁵³R. Kikuchi and K. Masuda-Jindo, *CALPHAD: Comput. Coupling Phase Diagrams Thermochem.* **26**, 33 (2002).
- ⁵⁴C. McCammon, J. Peyronneau, and J.-P. Poirier, *Geophys. Res. Lett.* **25**, 1589 (1998).
- ⁵⁵A. L. Ankudinov, B. Ravel, J. J. Rehr, and S. D. Conradson, *Phys. Rev. B* **58**, 7565 (1998).
- ⁵⁶P. Gütllich, R. Link, and A. Trautwein, *Mössbauer Spectroscopy and Transition Metal Chemistry* (Springer-Verlag, Berlin, 1978).
- ⁵⁷T. E. Cranshaw, *J. Phys. E* **7**, 122 (1974).
- ⁵⁸J. F. Lin, V. V. Struzhkin, S. D. Jacobsen, M. Y. Hu, P. Chow, J. Kung, H. Liu, H. K. Mao, and R. J. Hemley, *Nature (London)* **436**, 377 (2005).
- ⁵⁹T. Tsuchiya, R. M. Wentzcovitch, C. R. S. da Silva, and S. de Gironcoli, *Phys. Rev. Lett.* **96**, 198501 (2006).
- ⁶⁰W. Sturhahn, J. M. Jackson, and J.-F. Lin, *Geophys. Res. Lett.* **32**, L12307 (2005).
- ⁶¹H. Bolvin and O. Kahn, *Chem. Phys.* **192**, 295 (1995).
- ⁶²H. Köppen, E. W. Müller, C. P. Köhler, H. Spiering, E. Meissner, and P. Gütllich, *Chem. Phys. Lett.* **91**, 348 (1982).
- ⁶³F. K. Lotgering and A. M. Van Diepen, *J. Phys. Chem. Solids* **38**, 565 (1977).
- ⁶⁴M. N. Taran and G. R. Rossman, *Am. Mineral.* **87**, 1148 (2002).